Laser Trapping of Circular Rydberg Atoms

R. g. G Cortiñas, M. Favier, B. Ravon, P. Méhaignerie, Y. Machu, J. m. M Raimond, C. Sayrin, M. Brune

Laser Trapping of Circular Rydberg Atoms

R. G. Cortiñas,[1,*] M. Favier,[1,*] B. Ravon,[1] P. Méhaignerie,[1]
Y. Machu,[1] J. M. Raimond,[1] C. Sayrin,[1,†] and M. Brune[1]

[1] *Laboratoire Kastler Brossel, Collège de France, CNRS, ENS-Université PSL, Sorbonne Université, 11 place Marcelin Berthelot, F-75231 Paris, France*

(Dated: January 13, 2020)

Rydberg atoms are remarkable tools for quantum simulation and computation. They are the focus of an intense experimental activity mainly based on low-angular-momentum Rydberg states. Unfortunately, atomic motion and levels lifetime limit the experimental time-scale to about 100 µs. Here, we demonstrate two-dimensional laser trapping of long-lived circular Rydberg states for up to 10 ms. Our method is very general and opens many opportunities for quantum technologies with Rydberg atoms. The 10 ms trapping time corresponds to thousands of interaction cycles in a circular-state-based quantum simulator. It is also promising for quantum metrology and quantum information with Rydberg atoms, by bringing atom-field interaction times into unprecedented regimes.

Rydberg atoms have remarkable properties. Their long lifetimes, large sensitivities to external fields and huge dipole-dipole interactions have led to milestone developments in quantum simulation [1–4], quantum information [5], quantum optics [6–14], quantum sensing [15–17] and molecular physics [18, 19]. Most of these experiments use laser-accessible low-angular-momentum states, with a lifetime in the hundred microsecond range.

Circular Rydberg Atoms (CRAs) (maximal angular momentum, $\ell = |m| = n - 1$, $n \gg 1$ being the principal quantum number) have a much longer intrinsic lifetime, 30 ms for $n = 50$. This makes them ideal tools for cavity quantum electrodynamics (CQED) [20] or quantum-enabled sensing [16, 21]. Moreover, CRAs are utterly promising for building hybrid quantum systems with superconducting-circuit devices [22, 23], for Rydberg-constant metrology [24] and for quantum simulation with alkaline [25] or alkaline-earth atoms [26].

By significantly lengthening the interrogation times and by spatially localizing the atoms, trapping of Rydberg atoms [27] is instrumental for the development of quantum technologies using them. Circular Rydberg atoms have been magnetically trapped [28] at room temperature, with a black-body-radiation-reduced lifetime of a few hundred µs only. In addition, they suffer from decoherence induced by state-dependent magnetic potentials. For low-angular-momentum Rydberg states, early experiments have demonstrated laser- [29, 30] and electric-field [31–33] trapping. Recently, 3D ponderomotive laser traps [34] and optical tweezers [35] have been reported, with interesting perspectives for quantum simulation. However, the short lifetime of these low-ℓ Rydberg states and their high photoionization rate [36] limit the trapping time to, again, a few hundred µs. Laser-trapping of CRAs is thus highly desirable for Rydberg-based quantum technologies.

Here, we demonstrate laser trapping of circular Rydberg atoms in a cryogenic environment. We excite laser-cooled atoms to the $n = 52$ circular Rydberg level inside a hollow Laguerre-Gauss (LG) beam. These atoms are repelled by the laser-induced ponderomotive potential [27] and transversally confined in the light tube for times up to 10 ms. We measure a trapping frequency of 1.37 kHz. We check that the lifetime and the coherence of the trapped atoms are not measurably affected by the light, as expected for levels insensitive to photoionization [25] and for a nearly n-independent trapping potential [27].

The experimental setup is shown on Fig. 1(a). Rubidium-87 atoms are loaded in a 3D mirror-magneto-optical trap (MOT) formed in front of a Rubidium-coated mirror [37, 38] enclosed in a 4 K ^{4}He cryostat that shields the Rydberg atoms from room-temperature black-body radiation [39]. A molasses stage further cools the atoms down to $\simeq 10 - 20$ µK in their ground state $|5S_{1/2}, F = 2\rangle$. We excite the atoms into $|52D_{5/2}, m_J = 5/2\rangle$ by a 2 µs-long two-photon laser excitation [Fig. 1(b)]. It makes use of a 780 nm-wavelength red laser beam (100 µm diameter) perpendicular to the MOT mirror and of a 480 nm-wavelength blue laser beam (22 µm diameter) aligned with the x-axis [axes definition in Fig. 1(a)]. The two crossed beams define a cigar-shaped Rydberg cloud elongated along the x-direction. The red laser is blue-detuned from the intermediate $|5P_{3/2}, F' = 3, m_{F'} = 3\rangle$ level by $\Delta = 560$ MHz, while the frequency of the blue laser can be scanned around the two-photon resonance condition.

The excitation is performed in an $F = 0.8$ V/cm electric field along the y-axis, defined by the grounded MOT mirror and electrode V_s [Fig. 1(a)]. After the end of the laser pulses, we adiabatically transfer the atoms into the $n = 52$ circular state ($m = +51$, noted $|52C\rangle$), using microwave (mw) and radiofrequency (rf) transitions [39–41]. We measure the populations of individual Rydberg levels via state-selective field ionization. We apply, with electrode V_s, a 200 µs-long electric field ramp, which successively ionizes the Rydberg levels. The measurement distinguishes low-m levels from high-m levels with the same n and resolves levels with different

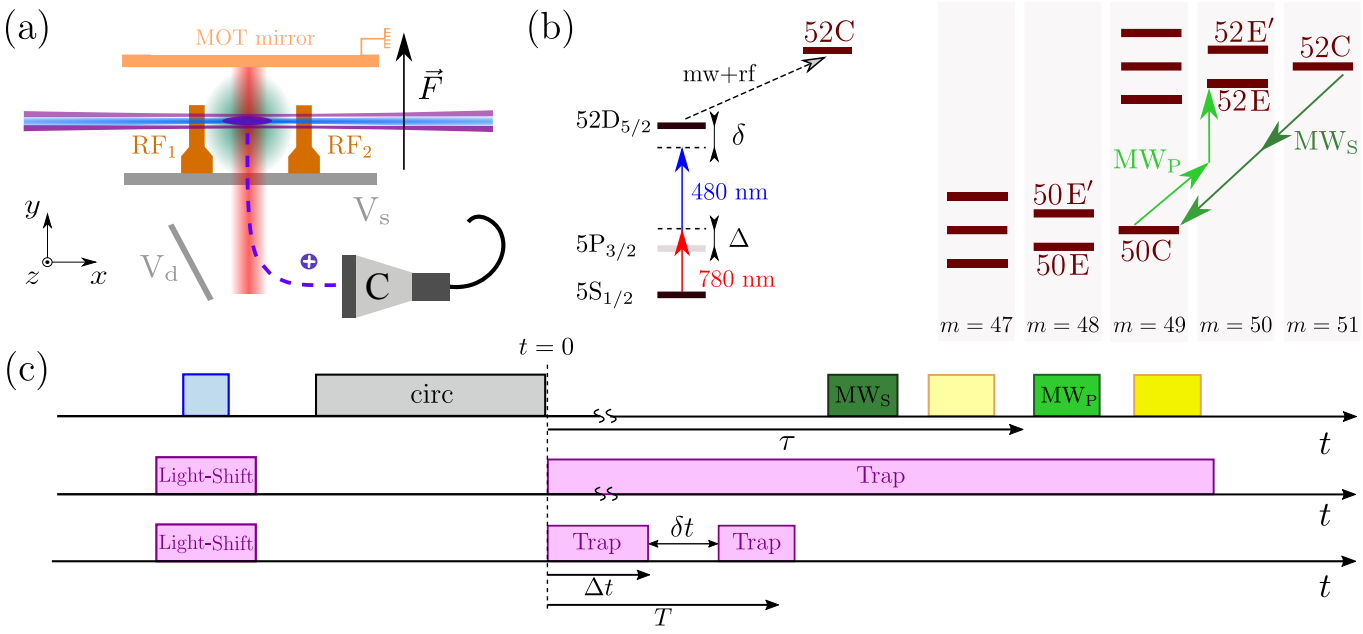

Figure 1. **(a) Experimental setup** with axes definition. The blue and red Rydberg excitation lasers cross in the cold atom cloud (green), about 4 mm away from the surface of the MOT mirror. The electrode V_s applies the electric field F and the ionization field. The Rb^+ ions (violet dashed line) are guided towards the channeltron C by the deflection electrode V_d. Four additional electrodes (only two, RF_1 and RF_2, are shown for clarity) apply the circular state preparation rf field and a static electric field gradient $\partial_z F$. The LG beam (purple) traps the Rydberg atoms (dark blue) **(b) Simplified level scheme.** Left: two-photon laser excitation (solid arrows) and circular state preparation (dotted arrow). Right: Partial diagram of the Stark levels in the $n = 50$ and $n = 52$ manifolds sorted by m values. The arrows represent the microwave transitions MW_S (level selection) and MW_P (probe). **(c) Timing of the experiment** (not to scale). Top frame: main events. From left to right: laser excitation (light blue), circular state preparation (grey), selection pulse MW_S (dark green), partial ionization (light yellow), probe pulse MW_P (dark green), field ionization (dark yellow). Middle frame: LG beam intensity versus time for the trapping experiment. Bottom frame: LG intensity for the trap oscillation-frequency measurement.

ns [41]. The resulting ions are counted in separate time windows. The circular state purity, measured by microwave spectroscopy, is $> 90\%$ [39]. The remaining population is distributed over a few high-m elliptical states ($n = 52, m \lesssim n - 2$).

We trap the CRAs in a ponderomotive trap acting on the almost-free Rydberg electron [27, 39]. Rydberg states are low-field seekers and are trapped in the local intensity minimum on the axis of a Laguerre-Gauss LG_{01} beam. We use a 1064 nm-wavelength fiber laser [42] and tailor it with a spatial light modulator (SLM) [43] into a LG beam [39]. It is sent onto the atoms along the x-axis [Fig. 1 (a)].

An intensity profile of the incoming trapping beam recorded outside the cryostat only gives a qualitative insight into the intensity distribution at the location of the atoms. Three successive thick glass windows on the cryostat vacuum tank and thermal shields appreciably distort the incoming beams. We probe *in situ* the trap beam intensity profile by measuring the light shifts it induces on the $|5S_{1/2}\rangle \rightarrow |52D_{5/2}\rangle$ ground-Rydberg transition [39]. Getting spectra for several positions of the trapping beam w.r.t. the blue beam, we reconstruct the LG beam intensity distribution. We use it to optimize the LG-beam shape, correcting with the SLM the aberrations introduced by the cryostat windows. Finally, the LG beam is found to be slightly elliptical with waists of 35 µm and 41 µm along the z- and y axes, respectively. The maximum light shift of the Rydberg excitation line is 3.8 MHz. The reconstructed peak laser intensity is thus $I = 6.6 \cdot 10^4$ W/cm^2 (total power 4.0 W), corresponding to a 80 µK trap depth, much larger than the initial atomic temperature.

The timing of the circular-atom trapping experiment is sketched in Fig. 1(c). We perform the Rydberg excitation with the trapping beam switched on for 15 µs around the 2 µs-long excitation pulse. We precisely center the LG beam on the axis of the blue laser by minimizing the observed light shift. Due to the finite size of the blue beam, the minimum average light shift is about 2 MHz. Setting the two-photon detuning from resonance, δ, to 0.5 MHz, the excitation selects, within the diameter of the blue laser, only atoms close the center of the LG beam. We estimate the transverse size of the initial Rydberg sample to be ~ 10 µm [39]. We switch off the trapping beam and perform in about 30 µs the transfer to the circular state, completed at time $t = 0$.

We then compare the spatial expansion of the Rydberg

atoms with and without the LG trapping beam, optionally switched on at $t = 0$. After a time delay τ, varying between 0.8 and 9.8 ms, we probe the Rydberg-atom spatial extension by mw spectroscopy. We monitor the broadening of a probe transition to a neighboring manifold, which experiences a linear Stark effect in an electric field gradient. It maps the Rydberg atoms positions onto their resonance frequencies.

For the larger τ values, blackbody-induced transfer of population from the initial $|52\mathrm{C}\rangle$ state to adjacent circular states (trapped as well in the LG beam) is significant. These transfers create a spurious background for the probe transition spectroscopy. In order to get rid of this background, we selectively transfer at time $\tau - 600$ µs all $|52\mathrm{C}\rangle$ atoms (irrespective of their position) into $|50\mathrm{C}\rangle$ by a 'hard' 0.8 µs-long microwave selection π-pulse $\mathrm{MW_S}$. After an additional 150 µs delay, we apply, during 160 µs, a partial ionization field ramp. It ionizes all Rydberg atoms with $n > 50$ and does not affect the population of $|50\mathrm{C}\rangle$. We apply, at $\tau - 200$ µs, a strong electric field gradient along the z-axis, $\partial_z F = 0.56\,\mathrm{V/cm^2}$, using the RF electrodes [Fig. 1(a)]. The gradients in the other directions are $\partial_x F = 0.18\,\mathrm{V/cm^2}$ and $\partial_y F = 0.10\,\mathrm{V/cm^2}$. We let the field relax to its steady-state ($F = 1.46\,\mathrm{V/cm}$) at $t = \tau$.

Finally, we apply at $t = \tau$ a 1.8 µs-long probe mw pulse $\mathrm{MW_P}$ on the $|50\mathrm{C}\rangle \rightarrow |52\mathrm{E}\rangle$ transition. The level $|52\mathrm{E}\rangle$ is the low-lying $|n, m = n - 2\rangle$ elliptical level, experiencing a first-order Stark shift of 99.8 MHz/(V/cm) (see level scheme in Fig. 1). A gaussian fit to the spectrum of this probe transition determines its Full Width at Half Maximum (FWHM), σ_P.

Figure 2(a) presents σ_P as a function of τ with (blue circles) and without (red squares) the trapping beam, and for two average Rydberg atom numbers in the sample at $t = 0$, $\bar{N} = \bar{N}_0$ (solid symbols) and $\approx \bar{N}_0/2$ (open symbols). Without trapping light, the Rydberg atoms move because of their finite temperature. When turning on the trapping laser, the linewidth remains basically constant. We only observe a slow broadening at long times resulting from the motion of the atoms along the unconfined x-axis in the electric field gradient $\partial_x F$.

The lines present a fit to the data with the predictions of a 3D (red) or 1D (blue) expansion model [39]. For the untrapped case, it is in excellent agreement with the observed data with a temperature of $T \approx 13.5$ µK, independently of $\bar{N}$. For the low-$\bar{N}$ trapped-atoms case (dotted blue line), we find $T = (14 \pm 3)$ µK. These temperatures are in good agreement with a direct time-of-flight measurement after the molasses stage. However, for the high-$\bar{N}$ trapped-atoms case (solid blue line), we find $T = (3 \pm 1)$ µK. This lower value of T may result from interactions between trapped CRAs, as explained below. Note that we never observe, within experimental noise, a wide pedestal on the trapped-atoms narrow line, which would be the signature of an untrapped fraction [39]. These data vividly demonstrate the main result of this paper: The atoms are trapped with a high efficiency and stay localized at the center of the trap for up to 10 ms.

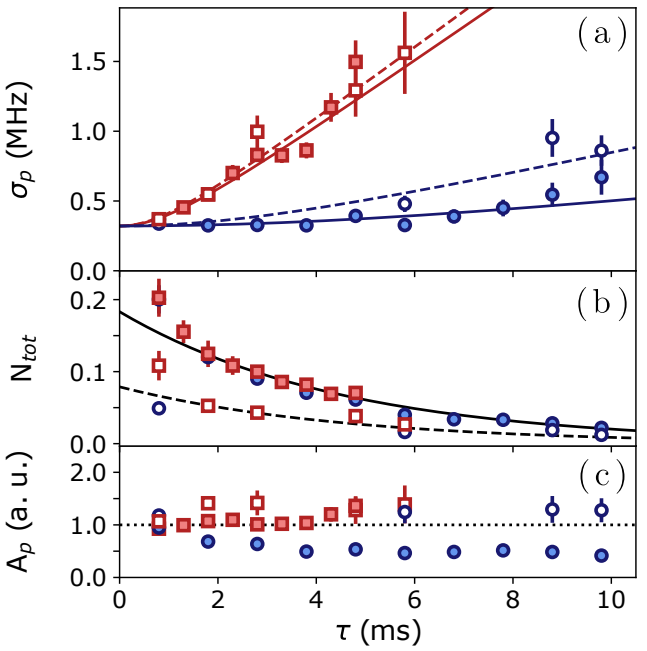

Figure 2. **Laser trapping.** (a) FWHM σ_P of the probe transition as a function of the delay time τ for untrapped (red rectangles) and trapped (blue circles) atoms. In all panels, full symbols correspond to an average atom number $\bar{N}_0$. Open symbols correspond to the same measurements with about $\bar{N}_0/2$ atoms. The lines result from a model of the Rydberg atoms expansion for untrapped (red) and trapped (blue) atoms, with $\bar{N} = \bar{N}_0$ (solid) or $\bar{N} \approx \bar{N}_0/2$ (dotted). (b) Total population of $|50\mathrm{C}\rangle$ at $t = \tau$, before the $\mathrm{MW_P}$ probe pulse for trapped (blue circles) and untrapped (red rectangles) atoms. The lines correspond to an exponential fit with a single decay time of $(4.6 \pm 0.3$ ms). The number of atoms at $t = 0$, uncorrected from detection efficiency, is $\bar{N} = \bar{N}_0 = 0.18 \pm 0.01$ for solid symbols and $\bar{N} = 0.08 \pm 0.01 \approx \bar{N}_0/2$ for open symbols. (c) Integrated area A_P of the $\mathrm{MW_P}$ probe spectrum for trapped (blue) and untrapped (red) atoms. Error bars correspond to 1-σ standard error deviation.

In Fig. 2 (b), we plot the total population in $|50\mathrm{C}\rangle$ at $t = \tau$, before $\mathrm{MW_P}$, for trapped (blue circles) and untrapped (red squares) atoms. In both cases, the population decay reflects the thermal transfers from the initial $|52\mathrm{C}\rangle$ state to neighboring circular states before the selection MW pulse ($\mathrm{MW_S}$). We observe no significant modification of the atomic lifetime when the trap is on. This shows that photoionization is quite negligible over this timescale, as expected [25].

Furthermore, we check that the purity of the circular states is not appreciably affected by the trapping. To this end, we plot the integrated area A_P of the recorded probe microwave spectrum as a function of τ, with and without

trapping light. A reduced A_P value indicates a transfer of population to other levels in the same manifold, which are not addressed by MW_P. The area A_P thus measures the purity of the circular levels, independently of their position in the electric field gradient. The results are shown in Fig. 2(c) for $\bar{N} = \bar{N}_0$ and $\approx \bar{N}_0/2$. For the lowest atom number, A_P is nearly constant for untrapped and trapped atoms, revealing that the trapping light does not affect the circular Rydberg level purity.

For the highest atom number, A_P is also constant in the untrapped case but decays rapidly (within 4 ms) to about half of its initial value for trapped atoms. This effect could be explained by the interactions between the trapped atoms. The 1D trap enhances the probability that two atoms come close enough to collide. These collisions may redistribute population in the Stark manifold. This would happen at a higher rate for faster atoms, explaining the rapid initial decay of A_P for the high $\bar{N}$ value, after which we expect that mainly slow atoms remain in $|52C\rangle$. It is consistent with the smaller effective temperature observed as compared to the lower $\bar{N}$ case. The low expansion temperature in Fig. 2(a) (solid blue circles) can thus be viewed as the harbinger of interatomic interactions of CRAs in the laser trap.

As a final check, we measure the CRAs trapping frequency [44]. The timing of the experiment is shown in Fig. 1(c). We move the trapping beam by 12 µm along the z-axis w.r.t. the blue laser. As before, the LG beam is on for 15 µs during Rydberg excitation. Setting the two-photon laser detuning to $\delta = 2.1$ MHz, about half of the light shift at maximum LG intensity, we excite Rydberg atoms on the inner slope of the LG beam [39]. After preparation of the circular states, we switch the trap on at time $t = 0$. The atoms start an oscillation along the z-axis at the trap frequency.

In order to probe this oscillation, we turn off the LG beam for $\delta t = 300$ µs after a variable waiting time Δt. Depending upon their velocity at Δt, the atoms can fly away from the trapping region. If it is not the case, we recapture them for a duration $T - \Delta t$, where $T = 2.6$ ms. We finally perform the detection sequence as above, setting MW_P at resonance with the $|50C\rangle \rightarrow |52E\rangle$ transition. The duration $T - \Delta t$ is chosen long enough so that the atoms flying away in the electric field gradient are impervious to MW_P. It thus addresses only those atoms that remained trapped.

In Fig. 3, we plot (blue circles) the number N_{52E} of atoms in $|52E\rangle$ as a function of Δt. We clearly observe damped oscillations. The recapture probability, and so N_{52E}, is lowest when the atoms are released at the time they speed through the bottom of the trap, *i.e.* when their kinetic energy is maximum. The population N_{52E} thus oscillates at twice the trapping frequency. From a fit of the signal (solid blue line), we extract a trap frequency of (1.37 ± 0.05) kHz. It is in fair agreement with a Monte-Carlo simulation of the anharmonic atomic

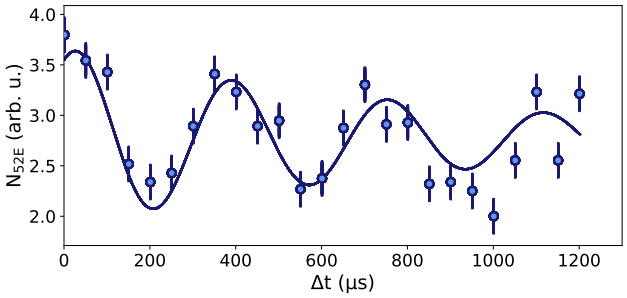

Figure 3. **Trap frequency measurement.** Blue circles with statistical error bars: number of atoms, N_{52E} in $|52E\rangle$, as a function of the time Δt at which the trap is switched off. Blue line: damped sinusoidal fit to the data.

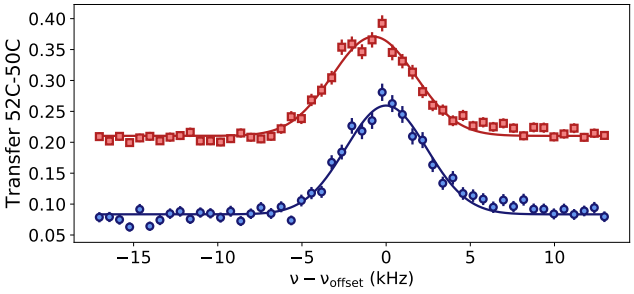

Figure 4. **Test of atomic coherence.** Microwave spectrum of the two-photon $|50C\rangle \rightarrow |52C\rangle$ transition for trapped (blue circles) and untrapped (red rectangles) atoms (statistical error bars) with $\nu_{\text{offset}} = 49.639071$ GHz. The fraction of atoms transferred to $|52C\rangle$ is plotted w.r.t. the detuning of the microwave source from resonance. The red points have been shifted upwards for clarity.

motion, which yields a frequency of 1.1 kHz. The discrepancy is attributed to drifts of the experimental setup and to rapid variations within the trapping-ligth intensity profile, which are not encompassed by the model [39].

Finally, we check that the coherence of the circular atoms is not affected by the trapping. We record, without applied field gradients, the spectrum of the nearly electric-field insensitive $|50C\rangle \rightarrow |52C\rangle$ transition driven by a 215 µs-long microwave pulse. Figure 4 shows the spectra obtained for untrapped (red squares) and trapped (blue circles) atoms. We observe a small (0.7 ± 0.2) kHz shift between the two situations, corresponding to a 1 mV/cm electric field drift over the one-hour data acquisition time, compatible with our experimental stability. The coherence-limited spectrum linewidth is probably determined by electric and magnetic field noises [41]. The FWHM of gaussian fits to the data (solid lines in Fig. 4) for untrapped and trapped atoms are respectively (5.8 ± 0.2) kHz and (5.7 ± 0.3) kHz. We thus observe, at the 200 Hz level, no effect of the trapping on the transition coherence, as expected for a level-independent trap-

ping potential.

We have demonstrated laser trapping of circular Rydberg atoms in two dimensions, for up to 10 ms. This time scale is currently limited only by the atomic lifetime in a finite-temperature environment. We have characterized the trapping potential and verified that it affects neither the circular levels lifetimes nor their coherence properties. The combination of the atom-loss-free 10 ms trapping time and of the 5 ms lifetime of the CRAs is unprecedented with respect to previous experiments [28, 32]. This timescale amounts to 1000 exchange-interaction cycles between two CRAs, with $n \sim 50$, held 5 µm apart. Extending this work to the optical trapping of CRAs in arrays of bottle-beam tweezers [35] would open new routes for quantum simulations, such as simulation over long time scales, relevant to problems such as quenches across quantum phase transitions and thermalization [25]. It would also be ideal for the development of quantum-enabled sensors based on CRAs or hybrid CQED experiments with Rydberg atoms and superconducting devices.

This work has been supported by the European Union FET-Flag project n°817482 (PASQUANS), ERC Advanced grant n° 786919 (TRENSCRYBE) and QuantERA ERA-NET (ERYQSENS, ANR-18-QUAN-0009-04), by the Region Ile-de-France in the framework of DIM SIRTEQ and by the ANR (TRYAQS, ANR-16-CE30-0026).

* These authors contributed equally to this work.
† Corresponding author: clement.sayrin@lkb.ens.fr

[1] H. Weimer, M. Müller, I. Lesanovsky, P. Zoller, and H. P. Büchler, A Rydberg Quantum Simulator, Nat. Phys. **6**, 382 (2010).
[2] H. Labuhn, D. Barredo, S. Ravets, S. de Léséleuc, T. Macrì, T. Lahaye, and A. Browaeys, Tunable Two-Dimensional Arrays of Single Rydberg Atoms for Realizing Quantum Ising Models, Nature **534**, 667 (2016).
[3] H. Bernien, S. Schwartz, A. Keesling, H. Levine, A. Omran, H. Pichler, S. Choi, A. S. Zibrov, M. Endres, M. Greiner, V. Vuletić, and M. D. Lukin, Probing Many-Body Dynamics on a 51-Atom Quantum Simulator, Nature **551**, 579 (2017).
[4] J. Zeiher, J.-Y. Choi, A. Rubio-Abadal, T. Pohl, R. van Bijnen, I. Bloch, and C. Gross, Coherent Many-Body Spin Dynamics in a Long-Range Interacting Ising Chain, Phys. Rev. X **7**, 041063 (2017).
[5] M. Saffman, T. G. Walker, and K. Mølmer, Quantum Information with Rydberg Atoms, Rev. Mod. Phys. **82**, 2313 (2010).
[6] M. D. Lukin, Colloquium: Trapping and Manipulating Photon States in Atomic Ensembles, Rev. Mod. Phys. **75**, 457 (2003).
[7] A. K. Mohapatra, T. R. Jackson, and C. S. Adams, Coherent Optical Detection of Highly Excited Rydberg States Using Electromagnetically Induced Transparency, Phys. Rev. Lett. **98**, 113003 (2007).
[8] T. Peyronel, O. Firstenberg, Q.-Y. Liang, S. Hofferberth, A. V. Gorshkov, T. Pohl, M. D. Lukin, and V. Vuletic, Quantum Nonlinear Optics with Single Photons Enabled by Strongly Interacting Atoms, Nature **488**, 57 (2012).
[9] S. Baur, D. Tiarks, G. Rempe, and S. Dürr, Single-Photon Switch Based on Rydberg Blockade, Phys. Rev. Lett. **112**, 073901 (2014).
[10] H. Gorniaczyk, C. Tresp, J. Schmidt, H. Fedder, and S. Hofferberth, Single-Photon Transistor Mediated by Interstate Rydberg Interactions, Phys. Rev. Lett. **113**, 053601 (2014).
[11] E. Distante, A. Padrón-Brito, M. Cristiani, D. Paredes-Barato, and H. de Riedmatten, Storage Enhanced Nonlinearities in a Cold Atomic Rydberg Ensemble, Phys. Rev. Lett. **117**, 113001 (2016).
[12] H. Busche, P. Huillery, S. W. Ball, T. Ilieva, M. P. A. Jones, and C. S. Adams, Contactless Nonlinear Optics Mediated by Long-Range Rydberg Interactions, Nat. Phys. **13**, 655 (2017).
[13] F. Ripka, H. Kübler, R. Löw, and T. Pfau, A Room-Temperature Single-Photon Source Based on Strongly Interacting Rydberg Atoms, Science **362**, 446 (2018).
[14] J. Li, M.-T. Zhou, C.-W. Yang, P.-F. Sun, J.-L. Liu, X.-H. Bao, and J.-W. Pan, Semideterministic Entanglement between a Single Photon and an Atomic Ensemble, Phys. Rev. Lett. **123**, 140504 (2019).
[15] J. A. Sedlacek, A. Schwettmann, H. Kübler, R. Löw, T. Pfau, and J. P. Shaffer, Microwave Electrometry with Rydberg Atoms in a Vapour Cell Using Bright Atomic Resonances, Nat. Phys. **8**, 819 (2012).
[16] A. Facon, E.-K. Dietsche, D. Grosso, S. Haroche, J.-M. Raimond, M. Brune, and S. Gleyzes, A Sensitive Electrometer based on a Rydberg Atom in a Schrödinger-Cat State, Nature **535**, 262 (2016).
[17] K. C. Cox, D. H. Meyer, F. K. Fatemi, and P. D. Kunz, Quantum-Limited Atomic Receiver in the Electrically Small Regime, Phys. Rev. Lett. **121**, 110502 (2018).
[18] V. Bendkowsky, B. Butscher, J. Nipper, J. P. Shaffer, R. Löw, and T. Pfau, Observation of Ultralong-Range Rydberg Molecules, Nature **458**, 1005 (2009).
[19] S. Hollerith, J. Zeiher, J. Rui, A. Rubio-Abadal, V. Walther, T. Pohl, D. M. Stamper-Kurn, I. Bloch, and C. Gross, Quantum Gas Microscopy of Rydberg Macrodimers, Science **364**, 664 (2019).
[20] S. Haroche, Nobel Lecture: Controlling Photons in a Box and Exploring the Quantum to Classical Boundary, Rev. Mod. Phys. **85**, 1083 (2013).
[21] E. K. Dietsche, A. Larrouy, S. Haroche, J. M. Raimond, M. Brune, and S. Gleyzes, High-Sensitivity Magnetometry with a Single Atom in a Superposition of Two Circular Rydberg States, Nat. Phys. **15**, 326 (2019).
[22] S. D. Hogan, J. A. Agner, F. Merkt, T. Thiele, S. Filipp, and A. Wallraff, Driving Rydberg-Rydberg Transitions from a Coplanar Microwave Waveguide, Phys. Rev. Lett. **108**, 063004 (2012).
[23] A. A. Morgan, V. Zhelyazkova, and S. D. Hogan, Preparation of Circular Rydberg States in Helium with $n \geq 70$ using a Modified Version of the Crossed-Fields Method, Phys. Rev. A **98**, 043416 (2018).
[24] A. Ramos, K. Moore, and G. Raithel, Measuring the Rydberg Constant Using Circular Rydberg Atoms in an Intensity-Modulated Optical Lattice, Phys. Rev. A **96**, 032513 (2017).

[25] T. L. Nguyen, J. M. Raimond, C. Sayrin, R. Cortiñas, T. Cantat-Moltrecht, F. Assémat, I. Dotsenko, S. Gleyzes, S. Haroche, G. Roux, T. Jolicœur, and M. Brune, Towards Quantum Simulation with Circular Rydberg Atoms, Phys. Rev. X **8**, 011032 (2018).

[26] J. Wilson, S. Saskin, Y. Meng, S. Ma, R. Dilip, A. Burgers, and J. Thompson, Trapped Arrays of Alkaline Earth Rydberg Atoms in Optical Tweezers, arXiv:1912.08754 [physics, physics:quant-ph] (2019), arXiv: 1912.08754.

[27] S. K. Dutta, J. R. Guest, D. Feldbaum, A. Walz-Flannigan, and G. Raithel, Ponderomotive Optical Lattice for Rydberg Atoms, Phys. Rev. Lett. **85**, 5551 (2000).

[28] D. A. Anderson, A. Schwarzkopf, R. E. Sapiro, and G. Raithel, Production and Trapping of Cold Circular Rydberg Atoms, Phys. Rev. A **88**, 031401 (2013).

[29] S. E. Anderson, K. C. Younge, and G. Raithel, Trapping Rydberg Atoms in an Optical Lattice, Phys. Rev. Lett. **107**, 263001 (2011).

[30] L. Li, Y. O. Dudin, and A. Kuzmich, Entanglement between Light and an Optical Atomic Excitation, Nature **498**, 466 (2013).

[31] C. Seiler, S. D. Hogan, H. Schmutz, J. A. Agner, and F. Merkt, Collisional and Radiative Processes in Adiabatic Deceleration, Deflection, and Off-Axis Trapping of a Rydberg Atom Beam, Phys. Rev. Lett. **106**, 073003 (2011).

[32] C. Seiler, J. A. Agner, P. Pillet, and F. Merkt, Radiative and Collisional Processes in Translationally Cold Samples of Hydrogen Rydberg Atoms Studied in an Electrostatic Trap, J. of Phys. B: At. Mol. Opt. Phys. **49**, 094006 (2016).

[33] V. Zhelyazkova, M. Žeško, H. Schmutz, J. A. Agner, and F. Merkt, Fluorescence-Lifetime-Limited Trapping of Rydberg Helium Atoms on a Chip, Mol. Phys. **117**, 2980 (2019).

[34] T. Graham, M. Kwon, B. Grinkemeyer, Z. Marra, X. Jiang, M. Lichtman, Y. Sun, M. Ebert, and M. Saffman, Rydberg-Mediated Entanglement in a Two-Dimensional Neutral Atom Qubit Array, Phys. Rev. Lett. **123**, 230501 (2019).

[35] D. Barredo, V. Lienhard, P. Scholl, S. de Léséleuc, T. Boulier, A. Browaeys, and T. Lahaye, Three-Dimensional Trapping of Individual Rydberg Atoms in Ponderomotive Bottle Beam Traps, arXiv:1908.00853 (2019).

[36] M. Saffman and T. G. Walker, Analysis of a Quantum Logic Device based on Dipole-Dipole Interactions of Optically Trapped Rydberg Atoms, Phys. Rev. A **72**, 022347 (2005).

[37] C. Hermann-Avigliano, R. C. Teixeira, T. L. Nguyen, T. Cantat-Moltrecht, G. Nogues, I. Dotsenko, S. Gleyzes, J. M. Raimond, S. Haroche, and M. Brune, Long Coherence Times for Rydberg Qubits on a Superconducting Atom Chip, Phys. Rev. A **90**, 040502 (2014).

[38] R. C. Teixeira, C. Hermann-Avigliano, T. L. Nguyen, T. Cantat-Moltrecht, J. M. Raimond, S. Haroche, S. Gleyzes, and M. Brune, Microwaves Probe Dipole Blockade and van der Waals Forces in a Cold Rydberg Gas, Phys. Rev. Lett. **115**, 013001 (2015).

[39] See supplementary metarials.

[40] R. G. Hulet and D. Kleppner, Rydberg Atoms in "Circular" States, Phys. Rev. Lett. **51**, 1430 (1983).

[41] To be published (2019).

[42] ALS-IR-74 from AzurLight Systems.

[43] LCOS-SLM X13138-03 from Hamamatsu.

[44] F. Nogrette, H. Labuhn, S. Ravets, D. Barredo, L. Béguin, A. Vernier, T. Lahaye, and A. Browaeys, Single-Atom Trapping in Holographic 2D Arrays of Microtraps with Arbitrary Geometries, Phys. Rev. X **4**, 021034 (2014).